Structural Characterization of Deep Sub-Micron Lithographic Structures using Small-Angle Neutron Scattering

Eric K. Lin[1], Ronald L. Jones[1], Wen-li Wu[1], John G. Barker[1a], Patrick J. Bolton[2], and George G. Barclay[2]

[1] Polymers Division and [1a] Center for Neutron Research, National Institute of Standards and Technology, Gaithersburg, MD 20899-8541.

[2] Shipley Company, Marlborough, MA 01752.

ABSTRACT

As critical dimensions continue to decrease with each technology node, the precise characterization of line width and profile becomes an increasingly challenging task. Small angle neutron scattering (SANS) offers several advantages for the characterization of sub-100 nm structures, particularly as a calibrating measurement method. In this work, SANS is used to characterize three samples prepared with the same mask and focus conditions, but different photoresist formulations. The mask pattern consists of parallel lines with a nominal line width of 180 nm and a 1:2 line to space ratio. Scattering data are taken using both a focused neutron beam instrument (two-dimensional data) and a perfect crystal diffraction ultra-high resolution small angle neutron scattering (USANS) instrument. From the location and intensity of observed diffraction peaks, both the periodicity of each grating pattern and the average line widths are determined from simple analytic expressions with nanometer resolution.

INTRODUCTION

High-resolution measurements of lithographic structures are needed as the critical dimensions of features continue to decrease to below 100 nm and resolution error budgets become increasingly stringent. Furthermore, both rapid characterization methods for on-line process monitoring and high-precision methods for absolute calibration purposes are needed. Current metrology techniques face difficult challenges to reach the required resolution for quantitative characterization at future technology nodes.

Microscopy-based methods such as scanning electron microscopy (SEM) [1-3] and atomic force microscopy (AFM) [4-6] are currently the most widely used methods for the characterization of feature critical dimension (CD) and line-edge roughness (LER). CD-SEM instruments rely on sophisticated edge detection algorithms for the analysis of top-down images to extract LER and line width variations. Cross-sectional images are also used to evaluate profile control and deviations from an ideal rectangular shape. The main limitations for SEM metrology are related to accurately deconvoluting the electron interaction with the sample. Further, a lack of a standard material has also limited the accuracy of SEM for absolute size determinations [3]. AFM measurements have recently been applied to characterize CD, cross-sectional profile, and sidewall roughness of lithographically prepared structures. For precise measurement, however, the tip shape must be well characterized in order to deconvolute its interaction with the structure and the tip must be narrow enough to sample areas within deep trenches between densely spaced structures. Other extensions have included the use of specially designed tips in order to better access the sidewall structure of high aspect ratio structures [4].

Diffraction-based methods such as optical scatterometry are also under development [7-10]. Scatterometry offers several advantages such as the possibility of high-throughput, non-destructive, and low cost CD evaluation. Modeling the observed scattered intensities, however, requires computationally intensive numerical solutions for Maxwell's equations with the rigorous coupled wave theory [11]. In addition, optical wavelengths are significantly larger than the structures to be measured and only the zero order diffraction intensities are accessible.

In each of the techniques mentioned above, complex modeling and tool development would be greatly enhanced with the existence of a standard technique with the capability of providing accurate information on standard samples. While neutron based techniques cannot be extended to on-line processing, due to the requirement of a high power neutron source, their applicability in the sub-100 nm regime provides an opportunity to further develop other techniques with on-line capabilities. Prior results from small angle neutron scattering (SANS) demonstrate the feasibility of neutron based probes in photoresist metrology [12, 13]. The advantages of the SANS measurement include: a) the transparency of silicon to neutrons allows measurement of structures without any additional sample preparation steps, b) a measurement metric averaged over an area of several square centimeters, providing information on process control over large length scales, c) increased applicability as critical dimensions decrease, and d) absolute length calibration with the neutron wavelength. In addition, unlike scatterometry methods, there are no concerns with shadowing from densely spaced structures or multiple organic layers in the film stack because SANS measurements are performed in transmission. Here, we report the results from SANS measurements of three parallel line grating patterns using both a SANS focusing lens configuration and a recently improved perfect-crystal diffraction for ultra-high resolution small angle neutron scattering (USANS).

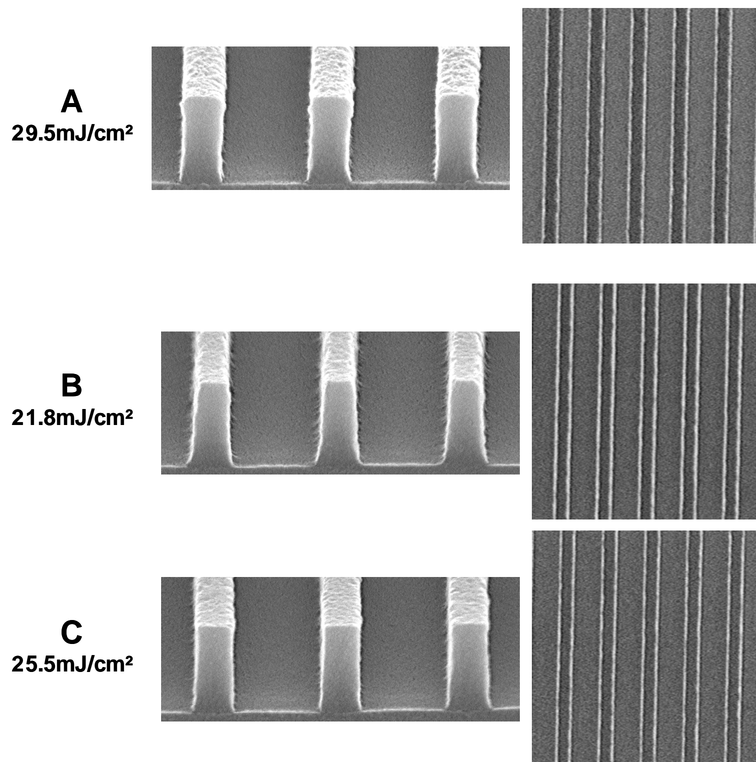

Figure 1. Side and top down SEM images of the three parallel line grating samples used in this study. Samples A, B, and C, have lines that are nominally 180 nm wide with a 1:2 line to space ratio. These structures were prepared using the same mask with exposure doses optimized for each photoresist formulation.

EXPERIMENT

Three parallel line grating patterns on 11 mm by 11 mm die areas were prepared on 200 mm silicon substrates for SANS measurements. Each pattern is fabricated using a different photoresist (A, B, or C) with the same mask, best focus conditions, and processing steps. The lines are nominally 180 nm wide, with a 1:2 line to space ratio. The film

thickness of the resist films was 4150 Å. The samples undergo a soft bake at 130 °C for 60 s, exposure to 248 nm DUV radiation with doses ranging from (21 to 30) mJ/cm^2, a post-exposure bake of 130 °C for 90 s, and development for 30 s in a standard developer solution. The SEM images of the structures are shown in Figure 1. In the SEM images, there are qualitative differences in the cross-sectional profile of the line structures with less visible variations in the critical dimension.

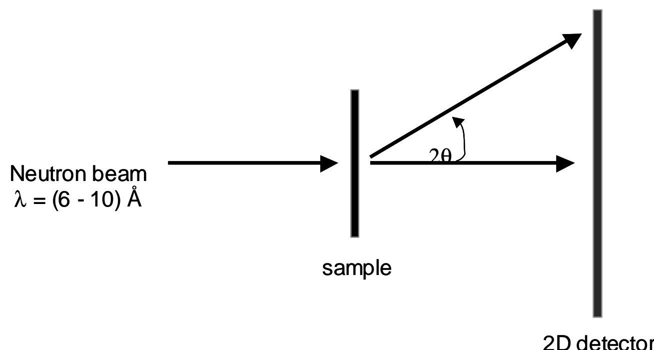

Figure 2. Schematic diagram of a top down view of the NG7 SANS experimental setup. The sample is placed directly into the beam normal to the incident beam. The sample may also be rotated relative to the incident beam to collect data from varying projections onto the detector providing more detailed information about the average line profile.

Two-dimensional SANS measurements were performed on the 30 m SANS NG7 instrument at the National Institute of Standards and Technology Center for Neutron Research (NCNR). A schematic diagram of a top-down view of the experimental configuration is shown in Figure 2. To access scattering angles needed to observe the first order diffraction peak from 5400 Å periodic structures, we used recently developed focusing optics consisting of a series of 28 biconcave MgF_2 lenses [14]. In this configuration, the neutron wavelength, λ, was 8.44 Å with a wavelength spread of $\Delta\lambda/\lambda = 0.11$. The sample to detector distance was 15.3 m and the final aperture size was 1.27 cm in diameter. The accessible range of q, ($q = (4\pi/\lambda)\sin\theta$, where 2θ is the scattering angle) is 0.0011 $Å^{-1}$ to 0.015 $Å^{-1}$. We reduce the two-dimensional scattering data with standard methods. The scattering data were placed on an absolute intensity scale using a secondary silica neutron scattering standard.

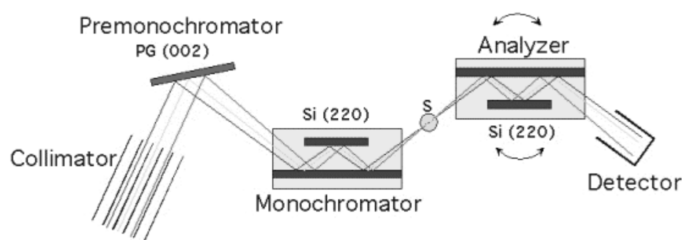

Figure 3. Schematic diagram of the PCD for USANS instrument at beamline BT5 at the NIST Center for Neutron Research. This is a Bonse-Hart type instrument with the sample placed between channel cut silicon (220) crystals used to provide ultra-high resolution in the scattering vector.

We also performed measurements on a recently improved perfect crystal diffractometer (PCD) for ultra-high resolution small angle neutron scattering [15, 16]. A schematic diagram of the instrumental configuration is shown in Figure 3. The USANS instrument is located on thermal neutron port BT5 at the NCNR. The PCD instrument uses a Bonse-Hart configuration with large channel-cut silicon (220) crystals as both monochromator and analyzer. The use of perfect crystals provides high angular resolution while multiple reflections define the beam such that the signal-to-noise ratio is improved to values comparable to those obtained with pinhole instruments like NG7. This instrument further

extends accessible angles for neutron scattering to lower q values. This instrument is capable of reaching a minimum q value of approximately 0.00005 $Å^{-1}$ corresponding to sizes approaching 10 μm. The neutron wavelength, λ, is 2.4 Å and the use of a perfect crystal diffractometer provides a narrow wavelength spread $\Delta\lambda/\lambda$ of approximately 0.04. The observable q range overlaps with the NG7 SANS measurement so that conventional SANS and USANS data may be compared and spliced together to probe the structure of materials over four orders of magnitude in size. Some of the disadvantages for the USANS measurement include the loss two-dimensional scattering data because of the need to scan over an angular range for the PCD configuration and significantly increased counting times.

For both instruments, the samples were placed directly into the neutron beam under ambient conditions as fabricated without any further preparation. The sample is mounted on a rotation stage so that the angle of the neutron beam on the sample can be controlled. The single crystal silicon wafer is essentially transparent to neutrons and almost all of the observed scattering intensity arises from the grating pattern. We observe significant scattering from a single layers 0.42 μm thick. For the SANS instrument, up to 4 h of counting time were used to obtain good statistics, but 10 min of counting time were sufficient to obtain useful data. For the USANS instrument, up to 12 h measurement times were required.

RESULTS AND DISCUSSION

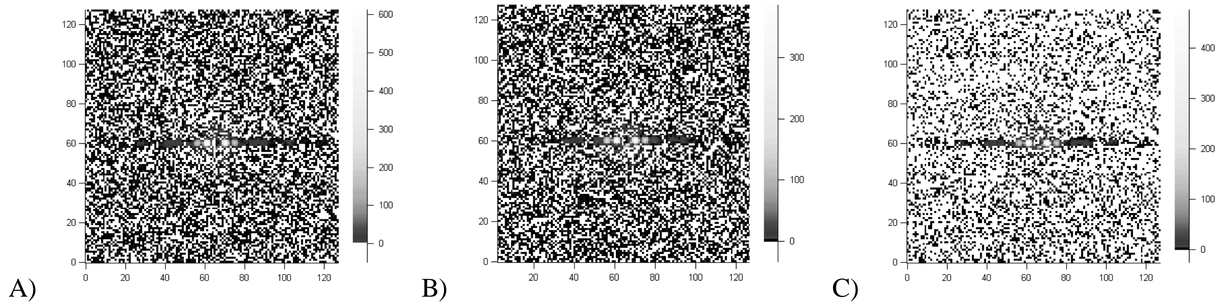

Figure 4. Two-dimensional SANS data from samples A), B), and C). The relative scattered intensity data are shown with background and empty beam scattering subtracted and on a linear scale. The lines are oriented vertically with respect to the detector resulting in diffraction spots in the horizontal plane of the detector. The diffraction spots are located near the beam center at very low scattering angles.

The two-dimensional SANS data are shown in Figure 4 after subtraction of background and open beam counts. The lines are oriented vertically with respect to the detector and diffraction spots are thus observed in the horizontal plane of the detector. For each sample, up to five orders of diffraction peaks are observed. The relatively large pattern sizes produce diffraction peaks in close proximity to the beam center, requiring the use of focusing lenses and restricting the optimization of neutron flux. Further reductions in critical dimensions will provide decreasing restrictions and shorter collection times. One-dimensional scattering curves are obtained by averaging over a narrow horizontal slice through the center of the detector. The curves are shown in Figure 5 and are vertically offset for clarity. diffraction spots appear as peaks at periodic q values reflective of the periodic grating structure. Although the line structures are nominally identical in size and appear very similar in the SEM images, the SANS data immediately reveal differences between photoresist formulations. The differences are in the relative intensities of the diffraction peaks as a function of q. For example, the data from samples A and C show an absence of a third order diffraction peak whereas sample B does have a third order peak, but is missing the fourth order diffraction peak. These differences are due to variations in the average feature shape or form of the line cross-section.

To mathematically describe the scattering data, the grating structures are represented in terms of the scattering length density, $\rho(z)$, as a convolution of a periodic grating function, $\delta(z)$, with the cross-sectional profile of a single line structure, $\Pi(H,L)$, or $\rho(z) = \delta(z)^* \Pi(H,L)$. $\Pi(H,L)$ is a square wave function with a height, H, and a half line width, L. A one-dimensional description for the real space model is sufficient because the lines are effectively infinitely parallel in the vertical direction of the detector.

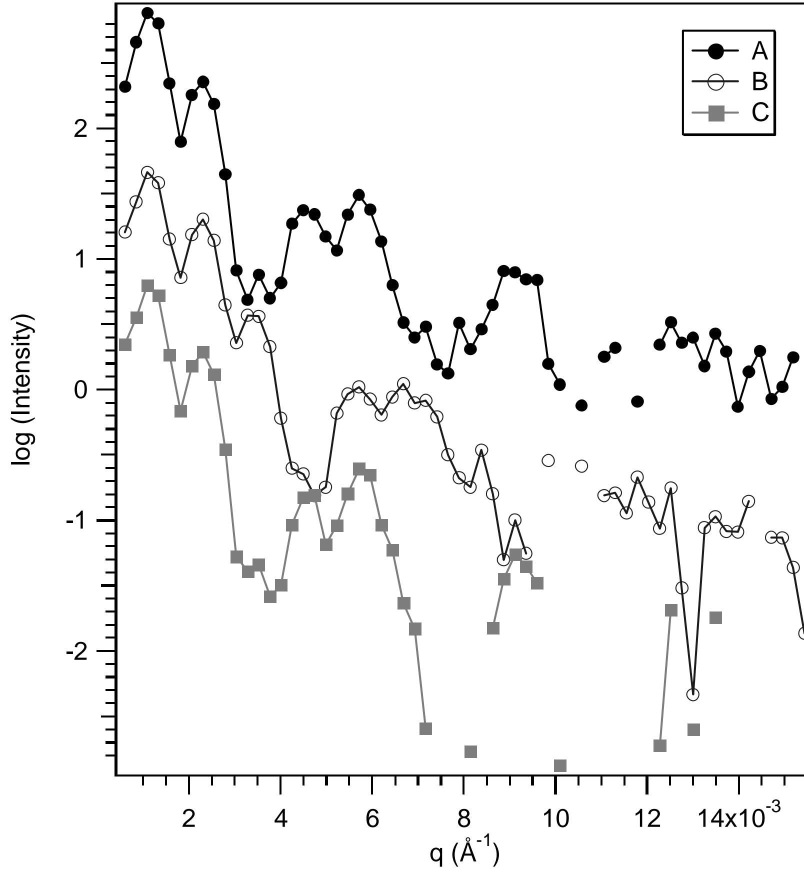

Figure 5. SANS data from samples A, B, and C averaged along the horizontal axis of the detector where the diffraction spots are located. The curves are offset for clarity. For samples A and C, the third order diffraction peak is missing whereas for sample B, the fourth order diffraction peak is missing. The peak intensities are related to the CD and the profile of an average line profile.

The scattered function, $A(q)$, is the Fourier transform of the convolution describing the real space profile. The Fourier transform of the grating function is a periodic grating function in Fourier space, $\delta(q)$, and the transform of the shape function, Π, is the form factor, $F(q)$. The functions are related through the expression, $A(q) = \delta(q)F(q)$ and the observed scattering intensities are given by $I(q) = \delta(q)F^2(q)$. The form factor function, $F(q)$, provides an envelope that modulates the intensities from peaks from the grating function. The observation of diffraction spots results from the highly periodic nature of the line structures and their intensity modulation allows for the quantitative characterization of their shape and size.

To account for variations in the line widths related to line-edge roughness, we introduce an additional convolution to the form of an individual line with a Gaussian function with a half width of ξ. The full width at half height of the line profile can then be approximated by the expression $2(L^2 + \xi^2)^{1/2}$. The magnitude of the parameter, ξ, provides a measure of line-edge roughness. The value of ξ does not necessarily correspond with LER values determined from SEM or AFM measurements. For the square wave function in this work, the square of the form factor $F^2(q)$ with the Gaussian roughness has a simple analytic form,

$$F^2(q) = 4H^2\left(\frac{\sin Lq}{q}\right)^2 \exp\left(-\frac{q^2\xi^2}{2}\right). \qquad (1)$$

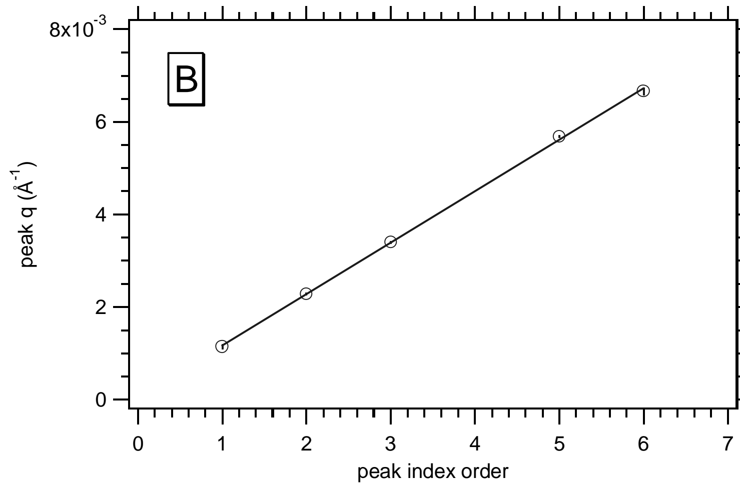

Figure 6. For sample B, the peak position is shown as a function of the diffraction peak index order. The fourth diffraction peak is not present because of a minimum in the form factor. A linear fit to the data provides a precise measurement of the periodicity of the grating pattern. The error bars are within the size of the symbols.

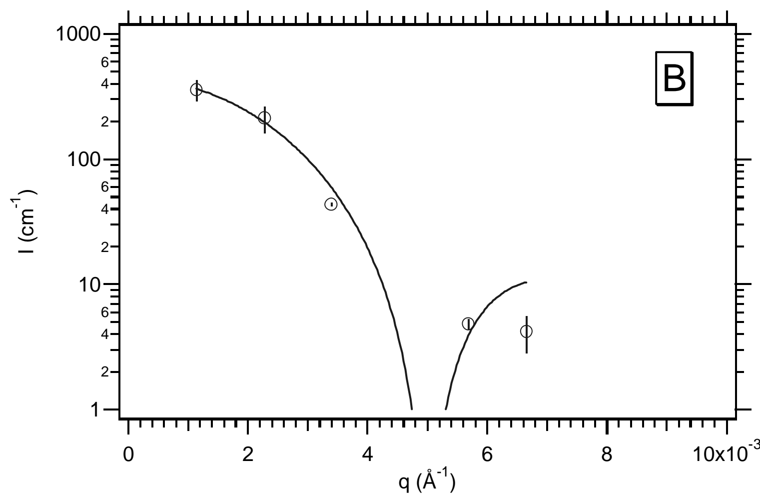

Figure 7. For sample B, the peak intensity is plotted as a function of the peak position. These intensities are proportional to the form factor of the line profile. A best fit to a smeared rectangular form factor function provides a measure of the line width and height of an average line.

The peak intensities and positions obtained from the SANS data are sufficient to quantify structural parameters using equation (1). In Figure 6, the diffraction peak position for sample B is plotted as a function of the peak order index. The slope of the best-fit line to the data provides an accurate measure of the periodicity of the diffraction grating. The periodicities are determined to be (5460 ± 95) Å, (5654 ± 72) Å, and (5420 ± 93) Å for samples A, B, and C, respectively [17]. The periodicities are very close to the designed value of 5400 Å, but variations are found between the samples. The periodicity of sample B is slightly larger than those of samples A and C. The measured quantities are absolute values because the length scales are determined by the neutron wavelength, a precisely known quantity, and not a secondary standard material or sample. In Figure 7, the peak intensities are plotted as a function of the peak position for sample B. The solid curve corresponds to a fit to the form factor expression from equation (1). For sample B, we

find that the average line width (2L) is (1256 ± 74) Å. The average widths for samples A and C are (1547 ± 30) Å and (1409 ± 52) Å, respectively. Samples A and C are similar in size, within 100 Å, but sample B is measurably smaller. These trends are qualitatively consistent with the cross-sectional SEM micrographs in Figure 1. The statistical measure of LER for this analytic expression, ξ, could not be determined definitively because the limited number of diffraction spots available precludes any sensitivity to fits to equation (1). Longer counting times may be necessary to collect better statistics from higher order diffraction peaks to better quantify ξ. The height of the structures, H, may also be used to provide relative measures of the heights of the three structures, assuming that the elemental composition of each photoresist formulation is similar. Sample A has the largest height and is normalized to 1.0. Relative to sample A, the fractional heights of samples B and C are (0.87 ± 0.08) and (0.91 ± 0.04), respectively. While sample A and C have the most similar line widths, samples B and C are closest in feature height.

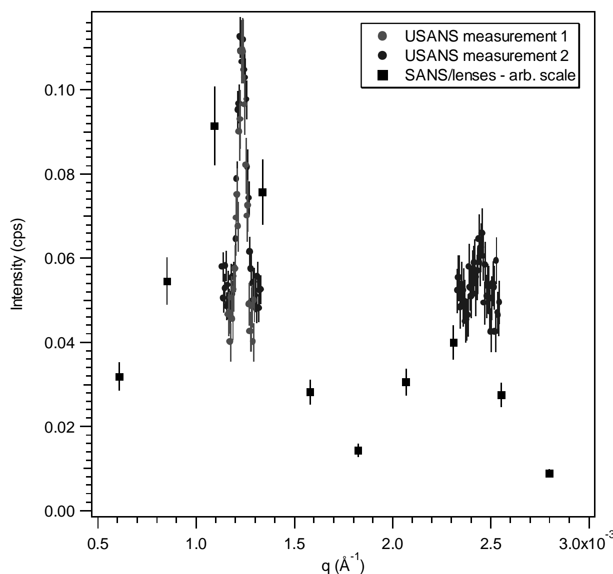

Figure 8. USANS data from the first two diffraction peaks from sample B along with data from the focused beam SANS configuration. The USANS diffraction peak widths are substantially narrower than the SANS peaks, but have a higher background count rate.

In the SANS configuration, the width of the diffraction peaks in the SANS measurement can be accounted for by the wavelength spread and the angular divergence of the beam. The USANS instrument has a smaller wavelength spread and much lower accessible q values. The USANS data from sample B are shown in Figure 8 along with the data from the SANS configuration. Only data about the first two orders of diffraction peaks were measured because of the long counting times needed for adequate statistics (1.3 h per point). Unfortunately, the background of the USANS instrument (approximately 0.052 counts/s) is larger than the signal expected from any higher order diffraction peaks from the sample. The narrower wavelength spread in the USANS instrument increases peak definition over the SANS instrument. The results in Figure 8 also show that the diffraction peak widths are accounted for by the wavelength spread (approximately 4 %). This illustrates the high quality of the structures fabricated on the silicon wafer, but precludes the use of the scattering data about the diffraction peak location to extract further information about the sample such as the sidewall roughness. The diffraction peaks from the two instruments do not overlap precisely, possibly due to difficulties in precise sample alignment in the USANS measurement. Sample alignment is more precise in the SANS configuration because of the availability of a two-dimensional detector and a sample rotation stage. In general, these initial results show that USANS and SANS may together be used to characterize structure over four orders of magnitude in size, providing the capability to study diffraction from large line to space ratios that may be representative of isolated line structures.

SUMMARY

SANS and USANS measurements have been performed on three parallel line grating patterns prepared with an identical mask and processing conditions but different photoresist formulations. SANS data are sufficient to distinguish nanometer differences in the grating periodicity, average line width, and the structure height, while USANS measurements probed the resolution limits of diffraction peak width. The width of the diffraction peaks remains limited by the wavelength spread. Future work will involve rotations of the samples to measure additional projections onto the detector to provide detailed information about line shape.

The high spatial resolution of the SANS methodology in characterizing the structure of deep sub-micron features provides several advantages. The measurements are non-destructive and can be performed on structures prepared directly on silicon substrates with simple analytic expressions describing the observed scattering patterns and intensities. While the requirement of a neutron source restricts its applicability, the potential to characterize sub-100nm structures with nanometer precision will allow the development of standard reference materials and the exploration of next-generation process-line characterization techniques.

ACKNOWLEDGEMENTS

We gratefully acknowledge significant technical assistance and insight from Charles J. Glinka, Derek Ho, Sung-min Choi and Paul Butler from the National Institute of Standards and Technology Center for Neutron Research.

REFERENCES

1. H. Marchman, in *Characterization and Metrology for ULSI Technology*, edited by D. G. Seiler, A. C. Diebold, W. M. Bullis, T. J. Shaffner, R. McDonald, and E. J. Walters (American Institute of Physics, College Park, MD, 1998), p. 491.
2. G. W. Reynolds and J. W. Taylor, *J. Vac. Sci. Technol. B,* **17**, 2723 (1999).
3. M. T. Postek, A. E. Vladar, S. N. Jones, and W. J. Keery, *Proc. SPIE*, **1926**, 268 (1993).
4. Y. Martin and K. Wickramasinghe, *Appl. Phys. Lett.*, **64**, 2498 (1994).
5. C. Nelson, S. Plamateer, and T. Lyszczarz, *Proc. SPIE*, **3332**, 19 (1998).
6. G. W. Reynolds and J. W. Taylor, *J. Vac. Sci. Technol. B*, **17**, 334 (1999).
7. C. J. Raymond, M. R. Murnane, S. Sohail H. Naqvi, and J. R. McNeil, *J. Vac. Sci. Technol. B*, **13**, 1484 (1995).
8. S. A. Coulombe and J. R. McNeil, *J. Opt. Soc. Am. A*, **16**, 2904 (1999).
9. I. Kallioniemi, J. Saarinen, and E. Oja, *Appl. Opt.*, **38**, 5920 (1999).
10. H. T. Huang, W. Kong, and F. L. Terry, *App. Phys. Lett.*, **78**, 3983 (2001).
11. T. K. Gaylord and M. G. Moharram, *Proc. IEEE*, **73**, 894 (1985).
12. W. L. Wu, E. K. Lin, Q. H. Lin, and M. Angelopoulos, *J. Appl. Phys.*, **88**, 7298 (2000).
13. E. K. Lin, W. L. Wu, Q. H. Lin, and M. Angelopoulos, *Proc. SPIE,* **4344**, 414 (2001).
14. S. M. Choi, J. G. Barker, C. G. Glinka, Y. T. Cheng, and P. L. Gammel, *J. Appl. Crystallogr.*, **33**, 793 (2000).
15. M. Agamalian, G. D. Wignall, and R. Triolo, *J. Appl. Cryst.*, **30**, 345 (1997).
16. A. R. Drews, J. G. Barker, C. J. Glinka, and M. Agamalian, *Physica B*, **241-243**, 189 (1998).
17. All data in the manuscript and in the figures are presented along with the standard uncertainty (±) of the measurement.